Synthetic analogs of active sites of iron-sulfur proteins: Bis(*o*-xylyldithiolato)ferrate(III) monoanion, a structurally unconstrained model for the rubredoxin Fe-S_4 unit*

(x-ray diffraction/iron-sulfur complexes/rubredoxin proteins)

R. W. LANE,† JAMES A. IBERS,§ R. B. FRANKEL,‡ AND R. H. HOLM†

† Department of Chemistry and ‡ Francis Bitter National Magnet Laboratory, Massachusetts Institute of Technology, Cambridge, Mass. 02139; and § Department of Chemistry, Northwestern University, Evanston, Illinois 60201

ABSTRACT **To complete the set of synthetic analogs of the three recognized types of active sites in iron-sulfur redox proteins, the compound $(Et_4N)[Fe((SCH_2)_2C_6H_4)_2]$, derived from *o*-xylyl-α,α'-dithiol, has been prepared and its structure has been determined by x-ray diffraction. The bischelate anion contains a near-tetrahedral Fe(III)-S_4 coordination unit with small rhombic distortions and all Fe-S bond distances in the range 2.252–2.279 Å. Its electronic properties have been partially characterized by measurement of electronic absorption, paramagnetic resonance, Mössbauer spectra, and magnetic susceptibility. The analog, as the protein, exhibits the Fe(III)/Fe(II) redox couple. These results substantiate designation of $[Fe((SCH_2)_2C_6H_4)_2]^-$ as a synthetic analog of the Fe(III)(S-Cys)$_4$ center in oxidized rubredoxin proteins. Comparison of the analog structure with that of the *Clostridium pasteurianum* rubredoxin active site shows that the former is substantially less distorted from idealized tetrahedral symmetry, and is considered to represent an essentially unconstrained structural model of the latter. Provided the grossly distorted tetrahedral stereochemistry of the protein site persists through final structural refinement, the analog–protein structural comparison supports an entatic state description of oxidized rubredoxin.**

Three types of active sites are currently recognized in nonheme iron-sulfur redox proteins (1–3). In terms of minimal composition they may be specified as Fe(S-Cys)$_4$ [rubredoxins (Rd)], Fe_2S_2*(S-Cys)$_4$ [plant, mammalian, and certain bacterial ferredoxins (Fd)], and Fe_4S_4*(S-Cys)$_4$ ["high-potential" (HP) proteins, 4- and 8-Fe bacterial proteins], in which S* is acid-labile or sulfide sulfur. The 1-Fe and 4-Fe sites have been defined by x-ray diffraction (4). In *Clostridium pasteurianum* oxidized rubredoxin (Rd_{ox}) the active site consists of a grossly distorted Fe(III)-S_4 tetrahedral unit with one unusually short Fe-S bond (4, 5). The structures of the active sites of *Chromatium* HP_{red} (6, 7) and *Peptococcus aerogenes* Fd_{ox} (4, 8) contain nearly equidimensional Fe_4S_4*S_4 clusters with substructural Fe_4S_4* cores having cubane-type stereochemistry. No x-ray structural information is available for any 2-Fe protein but a large body of physicochemical data (3) is entirely consistent with the indicated μ_2-sulfido structure. A common feature of all established or postulated active structures is approximate tetrahedral stereochemistry at the iron site(s). Recent research in these laboratories has demonstrated that the structures, many electronic properties, and ranges of oxidation states of the active sites of the lower molecular weight proteins can be closely approached or duplicated in relatively simple synthetic complexes derived from Fe(II,III), sulfide, and organic thiolates (9). The latter simulate coordination by cysteinyl residues. Thus $[Fe_4S_4(SR)_4]^{2-}$ (1) and $[Fe_2S_2(S_2\text{-}o\text{-xyl})_2]^{2-}$ (2), whose precise structures have been determined (10–12), have been shown to be synthetic analogs of the active sites of HP_{red} and 4- and 8-Fe Fd_{ox}, and 2-Fe Fd_{ox} proteins, respectively.

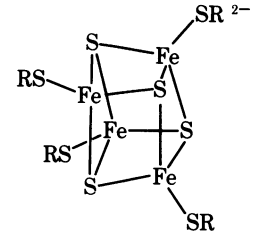

1

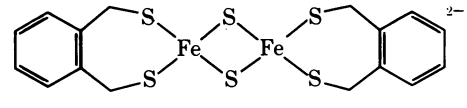

2

Heretofore absent from the analog-active site complementary pairs has been an isolable synthetic species compositionally related to the Rd active sites. Previously the only mononuclear tetrahedral Fe-S_4 species prepared have been $Fe[(SPMe_2)_2N]_2$ (13, 14) and [Fe(Boc-Gly(Cys-Gly-Cys)$_3$-Cys-Gly-NH_2)]$^{2-}$ (15), both of which contain Fe(II). The former, which lacks -CH_2S coordinating groups, has been isolated and structurally characterized, and the latter has been generated in solution but not isolated. Both serve as approximate electronic models for the Rd_{red} site but neither has as yet been reported to be oxidizable to an isolable or otherwise substantiated Fe(III) form. In view of the large and irregular departure of the Rd_{ox} active site from idealized T_d geometry, obtainment of an Fe(III) thiolate complex $[Fe(SR)_4]^-$ with unconstrained stereochemistry would provide further indication of the influence of protein structure and environment on stereochemical and attendant electronic properties of Fe-S protein active sites. We report here the synthesis and structural and partial electronic characterization of such a complex, bis(*o*-xylyldithiolato)ferrate(III) monoanion, $[Fe(S_2\text{-}o\text{-xyl})_2]^-$ This complex completes the set of analog-active site pairs which correspond to at least one oxidation level of each type of site.

Abbreviations: Fd, ferredoxin; HP, high-potential iron protein; Rd, rubredoxin; S_2-*o*-xyl, *o*-xylyldithiolate dianion; ox, oxidized; red, reduced; EPR, electron paramagnetic resonance.

* This is part XII of the series; part XI is ref. 12.

MATERIALS AND METHODS

Preparation of Compounds. All manipulations were performed under a pure dinitrogen atmosphere unless otherwise indicated; dry degassed solvents and freshly distilled *o*-xylyl-α,α'-dithiol (12) were employed.

(a) Tetraethylammonium bis(o-xylyldithiolato)ferrate(III). To a solution of *o*-xylyl-α,α'-dithiol (5.67 g, 33.4 mmol) and bis(tetraethylammonium)tetrachloroferrate(II) (5.09 g, 11.1 mmol) in a minimum volume of acetonitrile at 0° was added slowly with stirring 100 ml of a 0.67 M solution of sodium ethoxide in ethanol. The solution was warmed to room temperature and filtered. Exposure of the light brown filtrate to air immediately produced a purple solution and, shortly thereafter, a black crystalline precipitate which was isolated anaerobically, giving 2.8 g (50% yield) of product, $(Et_4N)[Fe(S_2\text{-}o\text{-}xyl)_2]$. The compound was further purified by recrystallization from hot acetone. *Analysis:* Calculated for $C_{24}H_{36}NS_4Fe$:C, 55.19; H, 6.90; N, 2.68; S, 24.53; Fe, 10.69. Found: C, 55.12; H, 6.80; N, 2.66; S, 24.39; Fe, 10.57.

(b) bis(Tetraethylammonium) tris(o-xylyldithiolato)diferrate(II). The preceding preparation, using 66 mmol of dithiol, 33 mmol of iron(II) salt, and 100 ml of a 1.32 M sodium ethoxide solution, was followed to the stage of the light brown filtrate. Removal of solvent under vacuum afforded a thick gummy material which was dissolved in about 250 ml of ethanol. This solution was filtered and crystallization began almost immediately in the filtrate. The product, $(Et_4N)_2[Fe_2(S_2\text{-}o\text{-}xyl)_3]$, was isolated as tan crystals (7.0 g, 50% yield) and was further purified by recrystallization from warm acetonitrile–ethanol. *Analysis:* Calculated for $C_{20}H_{32}NS_3Fe$: C, 54.77; H, 7.37; N, 3.19; S, 21.93; Fe, 12.73. Found: C, 54.70; H, 7.32; N, 3.07; S, 21.93; Fe, 12.65. Aeration of the filtrate from which this compound was isolated gave $(Et_4N)[Fe(S_2\text{-}o\text{-}xyl)_2]$. Both compounds should be handled in the absence of oxygen; the Fe(II) compound is especially oxygen-sensitive.

X-Ray Data and Structural Solution. $(Et_4N)[Fe(S_2\text{-}o\text{-}xyl)_2]$ was obtained as black rod-like crystals of noncentrosymmetric habit belonging to the orthorhombic system with space group C_{2v}^9-$Pn2_1a$. Cell dimensions are a = 13.413(8), b = 29.554(17), c = 13.448(10) Å, V = 5331 Å^3 [based on $\lambda(MoK_\alpha)$ = 0.70930 Å, t = 21.5°]. d_{calc} = 1.30 g/cm^3 for Z = 8; the experimental density was not determined owing to the air sensitivity of the compound. Eight formula units in the cell indicate two independent cations and two independent anions in the asymmetric unit. Linear absorption coefficient (Mo radiation) = 8.77 cm^{-1}. Transmission factors ranged from 0.732 to 0.801. The crystal used had the approximate dimensions 0.9 mm along the spindle axis (the [100] direction) × 0.3 mm × 0.3 mm. Particulars on methods of data collection, computer programs employed, sources of atomic scattering factors, and related matters have been given elsewhere (10, 11). A total of 6941 reflections was recorded, having the following distribution with respect to estimated standard deviations: $F_o^2 < 0$, 346; $0 \le F_o^2 \le \sigma$, 514; $\sigma \le F_o^2 \le 2\sigma$, 595; $2\sigma \le F_o^2 \le 3\sigma$, 523; $F_o^2 \ge 3\sigma$, 4963. These reflections include all those not forbidden by the space group and contain about 800 Friedel pairs of the type $hk\bar{l}$. The structure was solved by the usual combination of Fourier and least-squares techniques, following the initial successful trial structure found by direct methods. The refinement model included eventually anisotropic thermal parameters for all non-group, non-hydrogen atoms, and treated the four independent phenyl rings as rigid groups (D_{6h} symmetry, C-C = 1.392 Å) with individual isotropic thermal parameters. Refinement was by full-matrix least-squares methods minimizing $\Sigma\omega(|F_o|^2-|F_c|^2)^2$ and utilizing *all* 6941 $|F_o|^2$ reflections. This model involved 372 variables. The second anisotropic cycle yielded a difference Fourier map on which all H atom positions could be discerned. Methylene, methyl, and phenyl H atom positions were idealized (H-C-H = 109.5°, C-H = 0.95 Å). Isotropic thermal parameters of these H atoms were set at 1 Å^2 greater than the equivalent isotropic thermal parameter of the atom to which they are attached. These atoms were added as fixed contributions in the final cycles of refinement and their positions were recalculated once during the final three cycles. The final values of the agreement factors (on F_o^2) were R = 0.068 and R_w = 0.105. For the 4963 reflections having $|F_o|^2 \ge 3\sigma$ R (on F_o) = 0.045. The final error in an observation of unit weight was 1.78 e$^-$ and maximum density on the final difference Fourier map was 0.3 e$^-$/Å^3.

Magnetic susceptibilities were determined with a vibrating sample magnetometer and pure Ni metal calibrant. Electron paramagnetic resonance (EPR) spectra were measured with a Varian E-9 spectrometer operating at X-band frequencies. Electrochemical and Mössbauer measurements were made as previously described (16); half-wave and peak potentials at 25° are given in reference to a saturated calomel electrode.

RESULTS AND DISCUSSION

Description of the structure

Having established that the S_2-*o*-xyl ligand leads to tetrahedral stereochemistry around Fe(III) in **2**, this ligand, whose flexibility imposes no evident angular or distance constraints upon coordination, was utilized in the synthesis of the 1-Fe analog. Dithiolate ligands with shorter bite (S···S) distances are unsuitable in this respect (17, 18). The crystal structure of $(Et_4N)[Fe(S_2\text{-}o\text{-}xyl)_2]$ consists of discrete cations and anions. The former have the expected tetrahedral geometry and will not be discussed here. The two independent anions in the asymmetric unit have nearly identical structures. Each approaches T_d Fe-S_4 microsymmetry with small but definite rhombic distortions evident. The structures of the two anions are summarized by the following ranges and mean values of Fe-S distances and S-Fe-S angles: anion 1, 2.258(2)–2.279(2), 2.268 Å, 105.8(1)–112.6(1), 109.5°; anion 2, 2.252(2)–2.278(2), 2.267 Å, 106.7(1)–112.2(1), 109.4°. The overall structure and the Fe-S_4 coordination unit of $[Fe(S_2\text{-}o\text{-}xyl)_2]^-$ are displayed in Fig. 1; dimensions given are those for anion 1. The average dihedral angle between FeS_2 planes is 92.5°. The intrachelate bite distances and angles in the anions average to 3.736 Å, and 110.7°, respectively, and are close to the mean values in **2** (3.690 Å, 106.4°), indicating considerable similarity in the chelate ring structures of the two complexes. The chelate rings adopt non-planar chair-like conformations with obtuse dihedral angles between the mean least-squares planes FeS_2-C_2S_2 and C_2S_2-C_2Ph for the two anions falling in the ranges 126–140° and 108–111°, respectively. Consequently the complex is chiral, and the crystal selected for the x-ray investigation contained all anions with the same absolute configuration. The type of chirality encountered here, namely, that afforded solely by non-planar rings in what would otherwise be an achiral species, is most uncommon in metal chelate stereochemistry. The complex can be racemized by chair-boat-chair ring conformational changes, making improbable appreciable enantiomeric stability in solution.

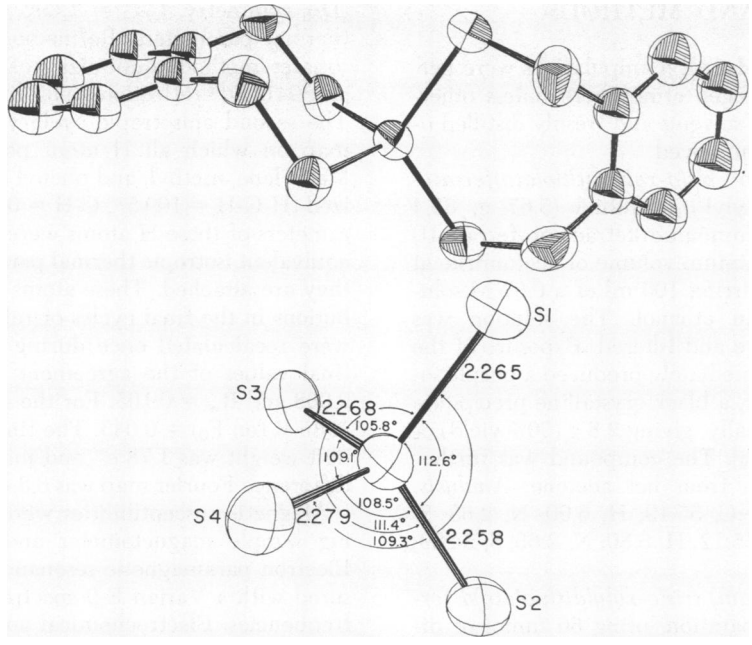

FIG. 1. Structure of the $[Fe(S_2\text{-}o\text{-}xyl)_2]^-$ anion; upper, overall structure (excluding H atoms) illustrating chair conformation of chelate rings and chiral stereochemistry; lower, dimensions of the Fe(III)-S_4 group in anion 1; Dimensions of this group in anion 2 are very similar to those shown. These groups have the same spatial orientation in the two drawings.

Electronic properties

In order to assess the electronic relationship between $[Fe(S_2\text{-}o\text{-}xyl)_2]^-$ and Rd_{ox} active sites, certain spectroscopic and magnetic properties are briefly compared.

(i) Absorption Spectra. Visible spectra of *Cl. pasteurianum* (19–21) and other Rd_{ox} proteins (22) are dominated by a three-band structure. The spectrum of the former is characterized by the following λ_{max} (ϵ_{mM}) data: 380 (10.9), 490 (8.9), about 580 nm (sh) (19, 20). The spectrum of $[Fe(S_2\text{-}o\text{-}xyl)_2]^-$ shown in Fig. 2 has principal bands at 354, 486, and 640–684 nm, which are considered to correspond to the protein features, albeit with somewhat reduced intensities and a pronounced red shift of the lowest energy bands. The latter effect is encountered in 2-Fe and 4-Fe analog spectra in nonaqueous media when compared to the spectra of the undenatured proteins (12, 23, 24). The reduced form of the analog, $[Fe(S_2\text{-}o\text{-}xyl)_2]^{2-}$, corresponding to the Rd_{red} site, is electrochemically detectable (*vide infra*) but has not been isolated. However, in experiments directed toward its synthesis the tetraethylammonium salt of an Fe(II) anion, whose analysis is consistent with the formulation $[Fe_2(S_2\text{-}o\text{-}xyl)_3]^{2-}$, was obtained. While the detailed structure of this complex is not known at present, the occurrence of a near infrared band at about 1930 nm is indicative of a tetrahedral Fe(II)-S_4 chromophore. This feature is assigned to the ligand field transition $^5E \rightarrow {}^5T_2$ from which the splitting parameter $\Delta_t = 5200\ cm^{-1}$, nearly the same as found for Rd_{red} (21) and the Fe(II) peptide complex (15) cited above. The solution spectrum provides no clear evidence for splitting of the $^5T_2$ state, which is quite substantial in Rd_{red} (21).

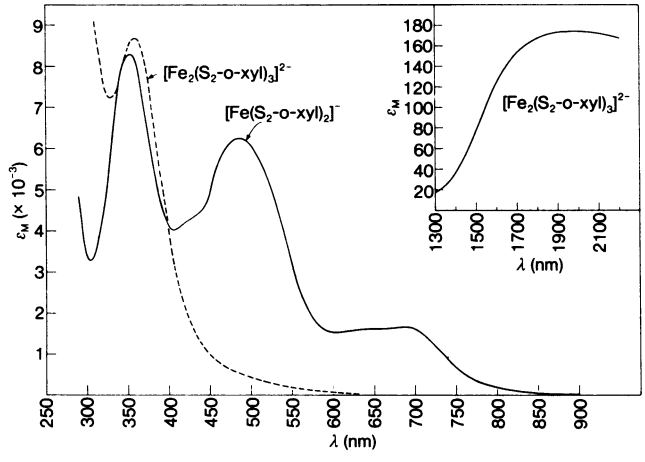

FIG. 2. Absorption spectra in dimethylformamide solution: $[Fe(S_2\text{-}o\text{-}xyl)_2]^-$ (—), $[Fe_2(S_2\text{-}o\text{-}xyl)_3]^{2-}$ (– – – –). Insert: near-infrared spectrum of $[Fe_2(S_2\text{-}o\text{-}xyl)_3]^{2-}$ in dimethylsulfoxide solution.

(ii) Magnetic and Mössbauer Properties. The sextet ground state required for tetrahedral Fe(III) was confirmed for $[Fe(S_2\text{-}o\text{-}xyl)_2]^-$. Magnetic susceptibilities in the solid state exhibited a T^{-1} dependence with the magnetic moments μ_{Fe} calculated from the Curie law ranging from 5.83 to 5.92 Bohr magnetons (BM) over the interval 60–292°K. For Rd_{ox} in solution $\mu_{Fe} = 5.85 \pm 0.20$ BM at 280–330°K (25). Mössbauer spectra were obtained for crystalline $(Et_4N)[Fe(S_2\text{-}o\text{-}xyl)_2]$ at 295, 77, and 4.2°K (Fig. 3) and for dimethylformamide and dimethylformamide/dichloromethane (3:1 v/v) frozen solutions of this compound. All spectra are quite similar and consist of single quadrupole doublets with a temperature-invariant quadrupole splitting $\Delta E_Q = 0.57 \pm 0.02$ mm/sec and isomer shift $\delta = 0.13 \pm 0.02$ mm/sec (relative to Fe metal). The line shape at 77°K is asymmetric with the low velocity component broader and less intense than the high velocity component; at 4.2°K the lines are more nearly symmetric. Application of longitudinal external magnetic fields H_0 up to 80 kOe at 4.2°K (Fig. 3) reveals that the sign of the principal component of the electric field gradient tensor is positive and that the magnetic splitting of the nuclear levels is due to the direct effect of the applied field and to a large field-dependent magnetic hyperfine interaction of opposite sign. For $H_0 = 80$ kOe this

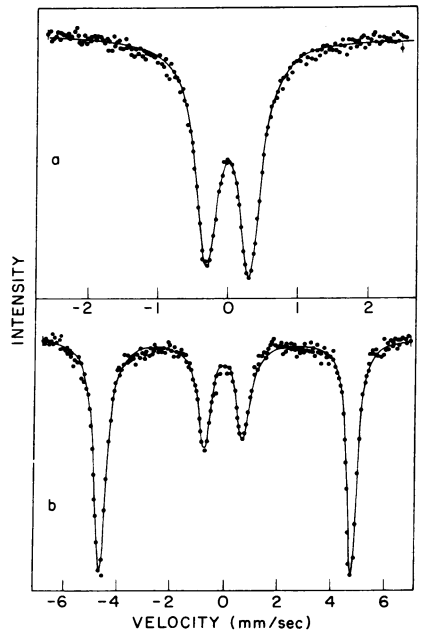

FIG. 3. Mössbauer spectra of $(Et_4N)[Fe(S_2\text{-}o\text{-}xyl)_2]$ at 4.2°K: (a) $H_0 = 0$; (b) $H_0 = 80$ kOe. The solid lines are theoretical least-squares fits to the data assuming Lorentzian line shapes. The source is ^{57}Co in Rh, also at 4.2°K.

interaction is equivalent to a magnetic field at the nucleus of −380 kOe.

The Mössbauer results are consistent with a high-spin Fe(III)-S_4 (16, 26) coordination unit distorted from T_d symmetry. Isomer shifts may be compared with $\delta = 0.25$ mm/sec for Rd_{ox} (77°K, room temperature source) (27, 28) and with values for other compounds containing similar units, e.g., 0.17, $CuFeS_2$ (29) and **2** (16), and 0.16 mm/sec, $KFeS_2$ (30). The high field saturation value of −380 kOe is quite close to that (−370 kOe) observed in Rd_{ox} at low temperature (25, 27, 28). These internal fields are reduced from the usual saturation value of about −500 kOe (31) found for Fe(III) with oxygen or nitrogen coordination, and presumably reflect the effects of spin depolarization and greater metal-ligand bond covalency. For example, a value of −380 kOe is observed in magnetically ordered $CuFeS_2$ at low temperature. The line shift asymmetries in the zero field spectra are ascribed to electron spin relaxation effects. The observation of greater asymmetry at 77°K compared to 4.2°K implies decreasing relaxation rate with increasing temperature, which can be understood in terms of zero field splitting of the sextet ground state into three Kramer's doublets (32).

The near identity of Mössbauer spectra observed in the crystalline state with those found in frozen solutions, including the magnetically perturbed spectrum in dimethylformamide/dichloromethane, implies that the solid and solution species are the same. EPR spectra of $[Fe(S_2\text{-}o\text{-}xyl)_2]^-$ in this and other frozen solutions reveal the sharp $g = 4.3$ signal found in the crystalline solid and generally indicative of high-spin rhombic Fe(III). Both the Mössbauer and EPR results demonstrate in particular that upon release from a crystalline environment the Fe-S_4 unit of $[Fe(S_2\text{-}o\text{-}xyl)_2]^-$ does not adjust to effective T_d or D_{2d} microsymmetry. EPR spectra of this complex observed at 1.5–140°K in several solvent media appear to be more complex than that of *Pseudomonas oleovorans* Rd_{ox} (33).

(iii) Voltammetry. In view of evidence adduced for the role of Rd as an electron carrier in the *P. oleovorans* ω-hydroxylase system (34) and numerous demonstrations of the reaction $Rd_{ox} + e^- \rightleftharpoons Rd_{red}$ *in vitro*, corresponding redox activity is a requisite property of any active site analog. Polarographic and cyclic voltammetric studies have demonstrated the reaction $[Fe(S_2\text{-}o\text{-}xyl)_2]^- + e^- \rightleftharpoons [Fe(S_2\text{-}o\text{-}xyl)_2]^{-2}$ in dimethylformamide solution. The cathodic polarogram consists of a single wave at $E_{1/2} = -1.03$ V, corresponding to a one-electron reduction. Slopes of plots of $\log[i/(i_d - i)]$ versus E are −57 mV (dropping mercury electrode) and −67 mV (Pt electrode), compared to the theoretical value of −59 mV for a reversible reaction. Current-voltage response curves elicited by cyclic voltammetry (Pt electrode) at scan rates of 10–500 mV/sec indicate that the redox process does not adhere to the diagnostic criteria for strictly reversible charge transfer (35), and the curves are in better accord with a kinetically quasi-reversible process. The near equality of cathodic and anodic peak currents ($i_{p,c}/i_{p,a} = 1.03 \pm 0.03$) over the scan range together with the polarographic results rule out irreversible charge transfer and substantiate the above mononuclear analog Fe(III)/Fe(II) redox couple. When *approximately* compared on a common potential scale (23, 24) the analog potential is about 600–700 mV more negative than proton values [E_0' about −0.04 to −0.06 V (19, 20, 34)]. Large cathodic shifts versus protein potentials are a common feature of all alkylthiolate analogs (12, 16, 23, 24) and represent influences of protein tertiary structure and active site environment which are not yet interpretable (23, 24).

Analog–protein structural comparison

The preceding results suffice to show that $[Fe(S_2\text{-}o\text{-}xyl)_2]^-$ and Rd_{ox} proteins contain similar chromophores, exhibit the same two oxidation levels, and possess high-spin Fe-S_4 coordination units which display rhombic departure from idealized tetrahedral symmetry in the crystalline phase and in frozen solutions and glasses. The high-spin spherically symmetric Fe(III) ion is devoid of ligand field stabilization effects on stereochemistry, and is expected to adopt a strictly regular coordination geometry in the absence of ligand structural constraints and the perturbing influences of crystalline packing forces and other medium effects. These factors, if operative, should afford mainly angular rather than distance distortions. An example is found in the precisely determined structure of $[PCl_4][FeCl_4]$ (36), whose anion deviates appreciably from T_d symmetry only by one angle about 5° larger than the other five (mean 108.6°). More extensive distortions are found in other salts of $[FeCl_4]^-$ (37). Other than noting that the largest S-Fe-S angle is the bite angle S(1)-Fe-S(2), the parameters in Fig. 1 do not reveal any clear-cut influence of chelate rings on the stereochemistry of the analog coordination unit, which is not subject to any crystallographically imposed symmetry requirements. While small crystalline and ligand perturbations cannot be completely discounted, $[Fe(S_2\text{-}o\text{-}xyl)_2]^-$ is considered to contain an essentially unconstrained Fe-S_4 unit whose stereochemistry should be closely approached in Rd_{ox} active sites in the absence of structural constraints imposed by protein.

The structure of *Cl. pasteurianum* Rd_{ox} has progressed through a series of refinement stages (38), with the latest published results obtained at 1.5 Å resolution (4, 5, 38). S-Fe-S bond angles range from 101(1) to 115(1)° and Fe-S bond distances are 2.34(2), 2.32(3), 2.24(3) and 2.05(3) Å. The latter is at least 0.17 Å shorter than any known Fe(III)-SR^- distance (Fig. 1; refs. 12, 17, and 39). If a comparison

between protein and analog structures is attempted by assigning to protein angles and distances uncertainties covered by three standard deviations, a distorted stereochemistry relative to $[Fe(S_2\text{-}o\text{-}xyl)_2]^-$ persists. Provided this situation obtains after final protein structural refinement [unpublished further refinement suggests that the short Fe-S distance may be lengthened by about 0.05 Å; K. D. Watenpaugh, L. C. Sieker, and L. H. Jensen, personal communication] and $[Fe(S_2\text{-}o\text{-}xyl)_2]^-$ is accepted as an unconstrained active site structural representation, the Rd_{ox} site may then be considered a well-defined case of the entatic state (40, 41). It has been cited as an example of an entatic condition suitable for facilitation of electron transfer (41), a proposal not inconsistent with the longer protein bond distances, which cover the range of Fe(III)-S and Fe(II)-S values determined for $[Fe(S_2\text{-}o\text{-}xyl)_2]^-$ and $Fe[SPMe_2)_2N]_2$ (14, mean 2.36 Å), respectively. This arrangement could conceivably reduce the enthalpic reorganization barrier for outer sphere electron transfer (42), and the short distance might provide a favored pathway for the transfer itself. It is our persuasion that demonstration of the entatic state in metalloproteins is best afforded by the type of analog–protein structural comparison offered here, which requires for completion the final results of the Rd_{ox} structural refinement. In this context synthetic analogs serve as symmetrized versions of active sites.

Lastly, while the final analog–protein comparison for 1-Fe coordination units may reveal a markedly irregular (entatic) stereochemistry in the latter, a similar situation does not seem likely to apply to 4-Fe active sites. The latest structural results for *Chromatium* HP_{red} (7) reveal near-perfect congruency between its $Fe_4S_4{}^*S_4$ cluster and that of its isoelectronic analog $[Fe_4S_4(SCH_2Ph)_4]^{2-}$ (10, 11). The high degree of analog–protein structural regularity arises in major part from the integral substructural $Fe_4S_4{}^*$ core common to both. While certain spectroscopic results suggest structural differences between HP_{red} and Fd_{ox}, and $[Fe_4S_4(SR)_4]^{2-}$ (43, 44), these differences are not clearly evident in the protein structures at their present stages of refinement. Judging from the comparative 1-Fe analog and Rd_{ox} active site stereochemistries, any such analog–protein structural variations are likely to be mainly confined to Fe–thiolate interactions external to the core, whose multiply bridged arrangement should be relatively more resistant to the impositions of protein structural effects.

This research was supported at M.I.T. and Northwestern University by National Institutes of Health Grants GM-19256 and HL-13157, respectively, and at the Francis Bitter National Magnet Laboratory by the National Science Foundation.

1. Orme-Johnson, W. H. (1973) *Annu. Rev. Biochem.* **42,** 159–204.
2. Hall, D. O., Cammack, R. & Rao, K. K. (1974) in *Iron in Biochemistry and Medicine,* eds. Jacobs, A. & Worwood, M. (Academic Press, New York), pp. 279–334.
3. Sands, R. H. & Dunham, W. R. (1975) *Quart. Rev. Biophys.* **7,** 443–504.
4. Jensen, L. H. (1974) *Annu. Rev. Biochem.* **43,** 461–474.
5. Jensen, L. H. (1973) in *Iron-Sulfur Proteins,* ed. Lovenberg, W. (Academic Press, New York), Vol. II, pp. 163–194.
6. Carter, C. W., Jr., Kraut, J., Freer, S. T. & Alden, R. A. (1974) *J. Biol. Chem.* **249,** 6339–6346.
7. Freer, S. T., Alden, R. A., Carter, C. W., Jr. & Kraut, J. (1975) *J. Biol. Chem.* **250,** 46–54.
8. Adman, E. T., Sieker, L. C. & Jensen, L. H. (1973) *J. Biol. Chem.* **248,** 3987–3996.
9. Holm, R. H. (1975) *Endeavour* **34,** 38–43.
10. Averill, B. A., Herskovitz, T., Holm, R. H. & Ibers, J. A. (1973) *J. Am. Chem. Soc.* **95,** 3523–3534.
11. Que, L., Jr., Bobrik, M. A., Ibers, J. A. & Holm, R. H. (1974) *J. Am. Chem. Soc.* **96,** 4168–4178.
12. Mayerle, J. J., Denmark, S. E., DePamphilis, B. V., Ibers, J. A. & Holm, R. H. (1975) *J. Am. Chem. Soc.* **97,** 1032–1045.
13. Davison, A. & Switkes, E. S. (1971) *Inorg. Chem.* **10,** 837–842.
14. Churchill, M. R. & Wormald, J. (1971) *Inorg. Chem.* **10,** 1778–1782.
15. Anglin, J. R. & Davison, A. (1975) *Inorg. Chem.* **14,** 234–237.
16. Mayerle, J. J., Frankel, R. B., Holm, R. H., Ibers, J. A., Phillips, W. D. & Weiher, J. F. (1973) *Proc. Nat. Acad. Sci. USA* **70,** 2429–2433.
17. Snow, M. R. & Ibers, J. A (1973) *Inorg. Chem.* **12,** 249–254.
18. Herskovitz, T., DePamphilis, B. V., Gillum, W. O. & Holm, R. H. (1975) *Inorg. Chem.* **14,** 1426.
19. Lovenberg, W. & Sobel, B. E. (1965) *Proc. Nat. Acad. Sci. USA* **54,** 193–199.
20. Lovenberg, W. & Williams, W. M. (1969) *Biochemistry* **8,** 141–148.
21. Eaton, W. A. & Lovenberg, W. (1973) in *Iron-Sulfur Proteins,* ed. Lovenberg, W. (Academic Press, New York), Vol. II, pp. 131–162.
22. Lode, E. T. & Coon, M. J. (1971) *J. Biol. Chem.* **246,** 791–802.
23. DePamphilis, B. V., Averill, B. A., Herskovitz, T., Que, L., Jr. & Holm, R. H. (1974) *J. Am. Chem. Soc.* **96,** 4159–4167.
24. Que, L., Jr., Anglin, J. R., Bobrik, M. A., Davison, A. & Holm, R. H. (1974) *J. Am. Chem. Soc.* **96,** 6042–6048.
25. Phillips, W. D., Poe, M., Weiher, J. F., McDonald, C. C. & Lovenberg, W. (1970) *Nature* **227,** 574–577.
26. Reiff, W. M., Grey, I. E., Fan, A., Eliezer, Z. & Steinfink, H. (1975) *J. Solid State Chem.* **13,** 32–40.
27. Rao, K. K., Evans, M. C. W., Cammack, R., Hall, D. O., Thompson, C. L., Jackson, P. J. & Johnson, C. E. (1972) *Biochem. J.* **129,** 1063–1070.
28. Thompson, C. L., Johnson, C. E., Dickson, D. P. E., Cammack, R., Hall, D. O., Weser, U. & Rao, K. K. (1974) *Biochem. J.* **139,** 97–103.
29. Raj, D., Chandra, K. & Puri, S. P. (1968) *J. Phys. Soc. Japan* **24,** 39–41.
30. Greenwood, N. N. & Whitfield, H. J. (1968) *J. Chem. Soc. A,* 1697–1699.
31. Freeman, A. J. & Watson, R. E. (1965) in *Treatise on Magnetism,* eds. Suhl, H. & Rado, G. (Academic Press, New York), Vol. IIA, pp. 167–305.
32. Blume, M. (1967) *Phys. Rev. Lett.* **18,** 305–308.
33. Peisach, J., Blumberg, W. E., Lode, E. T. & Coon, M. J. (1971) *J. Biol. Chem.* **246,** 5877–5881.
34. Lode, E. T. & Coon, M. J. (1973) in *Iron-Sulfur Proteins,* ed. Lovenberg, W. (Academic Press, New York), Vol. I, pp. 173–191.
35. Nicholson, R. S. & Shain, I. (1964) *Anal. Chem.* **36,** 706–723.
36. Kistenmacher, T. J. & Stucky, G. D. (1968) *Inorg. Chem.* **7,** 2150–2155.
37. Lauher, J. W. & Ibers, J. A. (1975) *Inorg. Chem.* **14,** 348–352.
38. Watenpaugh, K. D., Sieker, L. C., Herriott, J. R. & Jensen, L. H. (1973) *Acta Crystallogr. Sect. B* **29,** 943–956.
39. Koch, S., Tang, S. C., Holm, R. H., Frankel, R. B. & Ibers, J. A. (1975) *J. Am. Chem. Soc.* **97,** 916–918.
40. Vallee, B. L. & Williams, R. J. P. (1968) *Proc. Nat. Acad. Sci. USA* **59,** 498–505.
41. Williams, R. J. P. (1971) *Inorg. Chim. Acta Rev.* **5,** 137–155.
42. Jacks, C. A., Bennett, L. E., Raymond, W. N. & Lovenberg, W. (1974) *Proc. Nat. Acad. Sci. USA* **71,** 1118–1122.
43. Cerdonio, M., Wang, R.-H., Rawlings, J. & Gray, H. B. (1974) *J. Am. Chem. Soc.* **96,** 6534–6535.
44. Tang, S.-P. W., Spiro, T. G., Antanaitis, C., Moss, T. H., Holm, R. H., Herskovitz, T. & Mortenson, L. E. (1975) *Biochem. Biophys. Res. Commun.* **62,** 1–6.